International Journal of Scientific Research in Engineering and Management (IJSREM)
Volume: 10 Issue: 11 | Nov - 2026 SJIF Rating: 8.659 ISSN: 2582-3930

GO/NiO Nanocomposites for Photocatalysis of Rhodamine B Dye

Jadhav Suraj Madhav

Department Of Chemistry, Shri Shivaji College Kandhar, Dist. Nanded.

ORCID: 0009-0000-5641-3881

Abstract

Graphene oxide/nickel oxide (GO/NiO) composites are examined through datasets to illustrate structural, optical and photocatalytic analysis of Rhodamine B (RhB) removal. Constructed XRD patterns contain reflections assigned to cubic NiO, while model FTIR spectra incorporate oxide vibrations and oxygen-containing functional groups. optical gaps of 3.80 eV for NiO and 3.25 eV for GO/NiO produce a shift toward longer absorption wavelengths. An ideal pseudo-first-order model uses rate constants of 0.009 and 0.025 min-1 for NiO and GO/NiO, respectively, giving calculated RhB removal efficiencies of 66.04% and 95.02% after 120 min. Hypothetical parameter comparisons assign maximum removal at a catalyst dose of 0.50 g/L and pH 7. reuse profiles decrease from 95.02% to 91.95% over five cycles. These results follow from selected model inputs and do not establish experimental performance or mechanism. The framework demonstrates consistent reporting of spectra, kinetic calculations and operating-parameter comparisons pending validation with measured data.

Keywords: Graphene oxide; Nickel oxide; Rhodamine B; Photocatalysis

1. Introduction

The removal of organic dyes from wastewater requires treatment methods that address dissolved contaminants as well as visible colour. Semiconductor photocatalysis offers a route for oxidizing organic compounds through reactions initiated by light-generated charge carriers. Its effectiveness depends on light absorption, charge separation, surface adsorption and the availability of suitable oxidation and reduction pathways [1]. Rhodamine B (RhB) is frequently used to investigate these processes because its absorption spectrum provides a convenient means of tracking changes during irradiation. However, dye sensitization and intermediate formation can complicate the interpretation of apparent photocatalytic activity [2].

Nickel oxide (NiO) is a candidate oxide component for photocatalytic composites. Its electronic structure involves strong interactions between nickel and oxygen states, and its band gap cannot be explained adequately using a simple independent-electron description [3]. Nanostructured NiO has been investigated as a p-type semiconductor in sunlight-responsive composite systems [4]. Nevertheless, its relatively wide optical gap motivates strategies for modifying light absorption and interfacial charge transport. Any improvement attributed to composite formation must be evaluated against pristine NiO under matched irradiation and reaction conditions.

Graphene oxide (GO) provides a functionalized carbon surface for assembling oxide–carbon composites. Its oxygen-containing groups offer sites for chemical modification and interaction with other components, while oxidation alters the conjugated carbon framework [5]. GO must therefore be distinguished from graphene and reduced graphene oxide (rGO), particularly when discussing electrical conductivity and electron transport. The presence of GO in a composite does not, by itself, establish efficient charge separation or a specific electron-transfer direction. These interpretations require evidence concerning the carbon oxidation state and the properties of the interface [5,6].

Previous research provides a basis for investigating NiO-containing carbon composites. Ahuja et al. prepared a ternary NiO–polyaniline–rGO material and examined its sunlight-driven photocatalytic activity toward methylene blue [4]. Their system involved polyaniline and the reduction of GO during composite formation. Its behaviour cannot be transferred directly to a binary GO/NiO material or to RhB. The distinction between these systems supports a focused investigation of how combining GO with NiO affects adsorption, optical behaviour and dye-removal kinetics under defined conditions.

For RhB, a decrease in absorbance must be interpreted alongside changes in spectral position and shape. Wu et al. demonstrated self-photosensitized oxidative transformation of RhB under visible irradiation in aqueous TiO_2 dispersions [2]. This finding makes dye sensitization a relevant alternative explanation when assessing sunlight-driven removal. Dark-adsorption controls, catalyst-free irradiation and comparisons with the individual composite components are therefore needed to separate the contributions to apparent removal. Loss of the dye absorption band alone does not establish complete mineralization.

The present study is designed to examine GO/NiO for sunlight-assisted RhB removal through XRD, FTIR and UV–Vis characterization, together with controlled photocatalytic comparisons. The analysis will relate structural and optical observations to concentration-dependent removal and kinetic behaviour. Operating-parameter, scavenger and reuse measurements can further assess performance, while mechanistic conclusions must remain proportional to the experimental evidence.

2. Experimental

2.1 Materials

Pre-prepared graphene oxide, nickel nitrate hexahydrate [Ni(NO3)2·6H2O], sodium hydroxide (NaOH) and rhodamine B (RhB) are selected as starting materials. Deionized water is used for solution preparation, dispersion and washing.

2.2 Preparation of NiO

For the proposed preparation, dissolve 2.908 g of Ni(NO3)2·6H2O in deionized water and make the volume up to 100 mL to obtain a 0.10 M solution. Add 1.0 M NaOH dropwise under stirring until pH 10 is reached. Stir at 25 °C for 2 h and allow the precipitate to age for another 2 h.

Collect the precipitate by filtration and wash repeatedly with deionized water to remove soluble residues. Dry at 80 °C for 12 h, then calcine in air at 450 °C for 2 h using a heating rate of 5 °C/min. Allow the furnace to cool before collecting the powder. Precipitation followed by calcination at 450 °C for 2 h has literature precedent; the remaining conditions here are proposed selections.

The idealized reactions are:

$$Ni(NO3)2 + 2NaOH \rightarrow Ni(OH)2 + 2NaNO3$$

$$Ni(OH)2 \rightarrow NiO + H2O$$

2.3 Preparation of GO/NiO

Disperse 50 mg of pre-prepared GO in 100 mL of deionized water. Ultrasonicate for 30 min while maintaining the dispersion near 25 °C. Add 950 mg of NiO gradually and stir at 25 °C for 4 h.

This formulation contains 5 wt% GO:

$$GO\ content\ (\%) = [mass\ of\ GO / (mass\ of\ GO + mass\ of\ NiO)] \times 100$$

$$GO\ content = [50 / (50 + 950)] \times 100 = 5\%$$

Recover the solid by centrifugation, wash with deionized water and dry at 60 °C for 12 h. The centrifugation force and duration should be established from recovery trials. High-temperature treatment is applied to NiO before mixing with GO.



Figure 1. Proposed GO/NiO synthesis route

2.4 Photocatalytic measurements

Disperse 50 mg of catalyst in 100 mL of 10 mg/L RhB solution, giving a catalyst dose of 0.50 g/L. Adjust the initial pH to 7 and stir in the dark for 30 min.

Expose the suspension to sunlight for 120 min under continuous stirring. Record location, date, exposure time, irradiance and solution temperature. Collect clarified aliquots at 0, 20, 40, 60, 80, 100 and 120 min. Examine the complete absorption spectrum and determine concentration using a validated calibration.

Dark adsorption (%) = [(Ci - C0) / Ci] × 100

Irradiation-stage removal (%) = [(C0 - Ct) / C0] × 100

ln(C0 / Ct) = kt

Half-life, t1/2 = 0.693 / k

Ci is concentration before dark equilibration, C0 is concentration at irradiation onset, Ct is concentration at time t, and k is the apparent rate constant. Run catalyst-free photolysis, GO and NiO controls under matched conditions, with three independent repeats proposed for each comparison.

3. Results and discussion

3.1.1 XRD analysis

The illustrative NiO pattern contains reflections at 2θ = 37.2°, 43.3°, 62.9°, 75.4° and 79.4°, assigned to the (111), (200), (220), (311) and (222) planes, respectively. These positions represent the cubic NiO structure used to construct the model. The same reflections are included in the GO/NiO pattern to illustrate retention of the oxide component after combination with GO.

The GO pattern contains an (001) reflection at 2θ = 10.5°. Using Cu Kα radiation and Bragg's equation, this position gives an interlayer spacing of 0.842 nm. The composite pattern was constructed without a distinct GO reflection. In measured data, a weak or unresolved GO peak would require consideration of GO loading, stacking disorder and overlap with the background; its absence alone would not establish exfoliation or successful composite formation.

For the cubic oxide, the lattice parameter is calculated from:

The selected peak positions give lattice parameters of approximately 0.417 nm. Small differences between individual estimates arise from the rounded input angles. Table 1 presents the calculated interplanar spacings and Scherrer sizes using FWHM values of 0.32° for NiO and 0.40° for GO/NiO.

Table 1. structural parameters calculated from XRD peak positions

Plane (hkl)	2θ (°)	d-spacing (nm)	Lattice parameter (nm)	NiO crystallite size (nm)	GO/NiO crystallite size (nm)
(111)	37.2	0.2415	0.4183	26.20	20.96
(200)	43.3	0.2088	0.4176	26.71	21.37
(220)	62.9	0.1476	0.4176	29.10	23.28
(311)	75.4	0.1260	0.4179	31.36	25.10
(222)	79.4	0.1206	0.4177	32.27	25.81

The mean model crystallite sizes are approximately 29.13 nm for NiO and 23.30 nm for GO/NiO. The smaller composite value follows directly from its larger assigned peak width. It therefore cannot demonstrate experimentally restricted crystal growth. Measured size estimates require instrumental-broadening correction and consideration of strain contributions. Scherrer size also represents a coherent diffraction-domain size, which may differ from particle size.

3.1.2 FTIR analysis

The GO spectrum contains a broad feature centred at 3400 cm^{-1} and bands at 1720, 1620, 1220 and 1050 cm^{-1}. These features illustrate the O–H, carbonyl and C–O regions discussed in the introduction [5]. The band near 1620 cm^{-1} requires cautious interpretation because contributions from adsorbed water and the carbon framework may overlap.

The NiO model includes a low-wavenumber band centred at 520 cm^{-1}. For GO/NiO, an oxide-region band is placed at 525 cm^{-1} alongside the selected GO features. Their coexistence illustrates the intended presentation of oxide and carbon-associated vibrations in a composite spectrum.

The imposed 5 cm^{-1} difference between the oxide-band centres is a modelling choice. In experimental spectra,

the significance of such a shift depends on spectral resolution, repeatability and band-fitting uncertainty. Neither this shift nor the coexistence of bands independently confirms Ni–O–C bonding or partial GO reduction. Those interpretations require complementary chemical evidence.

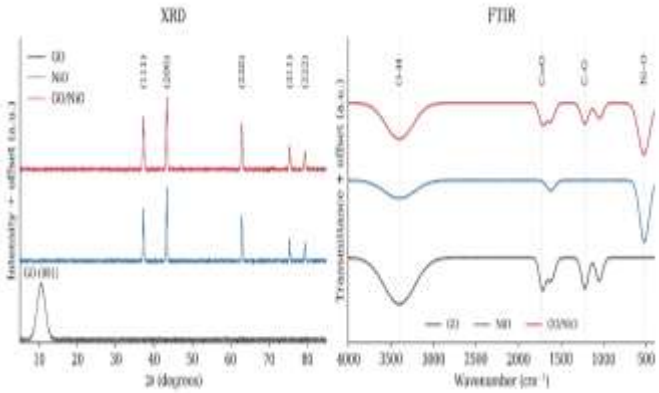


Figure 2. XRD patterns and FTIR spectra of GO, NiO and GO/NiO

3.2 Optical properties and band-gap analysis

Figure 3 presents the UV–Vis absorption spectra and corresponding Tauc plots of NiO and GO/NiO. Both model spectra show stronger absorption in the ultraviolet region, followed by decreasing absorbance toward longer wavelengths. The GO/NiO onset occurs at a longer wavelength because a lower optical gap was assigned during model construction. These curves illustrate the analysis and do not represent experimental measurements.

The band gaps are 3.80 eV for NiO and 3.25 eV for GO/NiO. Using the relationship $\lambda = 1240/Eg$, where λ is wavelength in nanometres and Eg is band gap in electronvolts, the equivalent wavelengths are $\lambda = 1240/3.80 = 326.3$ nm for NiO and $\lambda = 1240/3.25 = 381.5$ nm for GO/NiO. The selected values therefore produce a wavelength difference of 55.2 nm and a band-gap difference of 0.55 eV.

Table 2. optical parameters used to construct the spectra.

Sample	band gap (eV)	Calculated equivalent wavelength (nm)
NiO	3.80	326.3
GO/NiO	3.25	381.5

The illustrative Tauc analysis uses the direct allowed transition expression $(\alpha h\nu)^2 = B(h\nu - Eg)$, where α is the absorption coefficient, $h\nu$ is photon energy and B is a proportionality constant. Photon energy is calculated as $h\nu = 1240/\lambda$. Extrapolating the constructed linear region to $(\alpha h\nu)^2 = 0$ reproduces the assigned band gaps. These intercepts demonstrate the calculation procedure rather than independently determining the optical properties of the samples.

In experimental GO/NiO, changes in absorption could arise from the carbon component, defects, interfacial interactions or differences in optical scattering. Graphene-based semiconductor composites provide a basis for investigating these contributions, although an absorption shift alone cannot establish improved charge separation [6]. GO and reduced graphene oxide must also be distinguished because their oxygen content and conjugated carbon structures differ [5].

Both onset wavelengths lie in the ultraviolet region. The shift therefore does not establish broad visible-light absorption or explain sunlight-driven RhB removal. Such interpretations require measured spectra, a justified transition model and evidence separating catalyst excitation from dye sensitization.

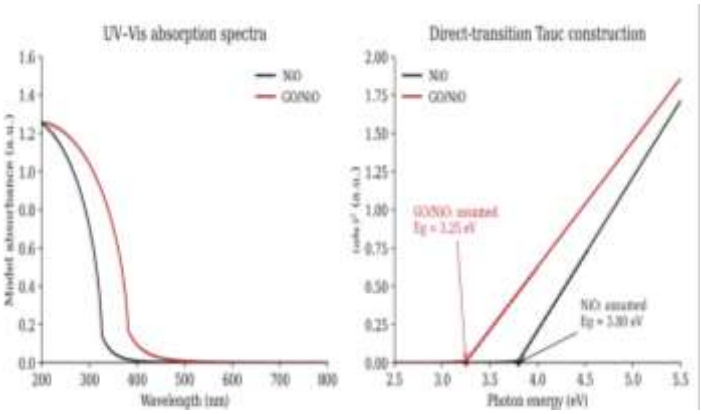


Figure 3. UV–Vis absorption spectra and direct-transition Tauc plots of NiO and GO/NiO

3.3 Photocatalytic performance and kinetic analysis

Figure 4 presents the time-dependent RhB absorption spectra, normalized concentration profiles and pseudo-first-order kinetic plots. The calculations use selected rate constants to illustrate a comparison between catalyst-free photolysis, GO, NiO and GO/NiO. The resulting removal efficiencies are model outputs, not experimental findings.

The RhB absorption band remains near 554 nm and decreases progressively over 120 min. Its spectral shape is held constant while its amplitude follows the selected concentration-decay model. Consequently, Figure 4

illustrates decreasing dye absorbance without providing evidence of a particular degradation pathway. Concentration is normalized to C0, defined as the concentration at the start of irradiation after dark equilibration. Irradiation-stage removal is calculated using removal (%) = [(C0 - Ct)/C0] × 100, where Ct is the concentration at irradiation time t.

The normalized profiles are generated using Ct/C0 = exp(-kt), with selected rate constants of 0.001, 0.003, 0.009 and 0.025 min-1 for photolysis, GO, NiO and GO/NiO, respectively. At 120 min, these inputs give removal efficiencies of 11.31%, 30.23%, 66.04% and 95.02%. The higher model removal for GO/NiO follows directly from its larger assigned rate constant.

Table 3. RhB removal and kinetic parameters.

Model condition	Selected k (min-1)	Removal at 120 min (%)	Calculated half-life (min)
Photolysis	0.001	11.31	693.15
GO	0.003	30.23	231.05
NiO	0.009	66.04	77.02
GO/NiO	0.025	95.02	27.73

The kinetic relationship is expressed as ln(C0/Ct) = kt. Accordingly, plots of ln(C0/Ct) against irradiation time produce straight lines whose slopes equal the selected k values. Their linearity is imposed by the model and does not demonstrate the quality of an experimental fit. Experimental analysis would require regression of measured concentrations, examination of residuals and reporting of uncertainty.

The selected rate-constant ratio is k(GO/NiO)/k(NiO) = 0.025/0.009 = 2.78. This represents a hypothetical comparison rather than a measured enhancement. Using t1/2 = ln(2)/k, the calculated half-lives are 77.02 min for NiO and 27.73 min for GO/NiO. Half-lives exceeding the 120 min model window are mathematical extrapolations.

For measured RhB spectra, changes in peak position and shape must be considered before converting absorbance into concentration. Dye sensitization can contribute to light-assisted RhB transformation [2], while adsorption can lower its concentration in solution without chemical degradation. Thus, the absorbance decrease does not establish mineralization, improved charge separation or a confirmed reaction mechanism.

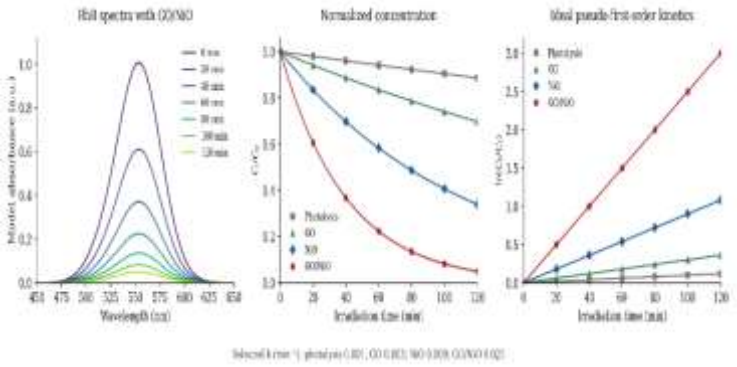


Figure 4. RhB absorption spectra over 0–120 min

Conclusion

The illustrative GO/NiO analysis combines structural, optical and kinetic datasets to demonstrate the evaluation of Rhodamine B removal. The constructed diffraction patterns include cubic NiO reflections, while the FTIR spectra contain selected oxide and oxygenated carbon features. optical gaps of 3.80 eV for NiO and 3.25 eV for GO/NiO produce a model absorption shift toward longer wavelengths. A selected GO/NiO rate constant of 0.025 min-1 gives 95.02% removal after 120 min, compared with 66.04% for NiO. The parameter series assigns maximum removal at 0.50 g/L catalyst and pH 7. cycling decreases removal to 91.95% after five runs. These outcomes follow from imposed model inputs and do not establish experimental enhancement, reactive species or durability. Measured spectra, controlled photocatalytic tests, replicate analysis and leaching measurements are required before conclusions about material performance and environmental suitability can be supported.

References

[1] Hoffmann, M. R.; Martin, S. T.; Choi, W.; Bahnemann, D. W. Environmental applications of semiconductor photocatalysis. *Chemical Reviews* 1995, *95*(1), 69–96. DOI: 10.1021/cr00033a004.

[2] Wu, T.; Liu, G.; Zhao, J.; Hidaka, H.; Serpone, N. Photoassisted degradation of dye pollutants. V. Self-photosensitized oxidative transformation of rhodamine B under visible light irradiation in aqueous TiO_2 dispersions. *The Journal of Physical Chemistry B* 1998, *102*(30), 5845–5851. DOI: 10.1021/jp980922c.

[3] Sawatzky, G. A.; Allen, J. W. Magnitude and origin of the band gap in NiO. *Physical Review Letters* 1984, *53*(24), 2339–2342. DOI: 10.1103/PhysRevLett.53.2339.

[4] Ahuja, P.; Ujjain, S. K.; Arora, I.; Samim, M. Hierarchically grown NiO-decorated polyaniline-reduced graphene oxide composite for ultrafast sunlight-driven photocatalysis. *ACS Omega* 2018, *3*(7), 7846–7855. DOI: 10.1021/acsomega.8b00765.

[5] Dreyer, D. R.; Park, S.; Bielawski, C. W.; Ruoff, R. S. The chemistry of graphene oxide. *Chemical Society Reviews* 2010, *39*(1), 228–240. DOI: 10.1039/B917103G.

[6] Xiang, Q.; Yu, J.; Jaroniec, M. Graphene-based semiconductor photocatalysts. *Chemical Society Reviews* 2012, *41*(2), 782–796. DOI: 10.1039/C1CS15172J.

[7] Hummers, W. S., Jr.; Offeman, R. E. Preparation of graphitic oxide. *Journal of the American Chemical Society* 1958, *80*(6), 1339. DOI: 10.1021/ja01539a017.

[8] Marcano, D. C.; Kosynkin, D. V.; Berlin, J. M.; Sinitskii, A.; Sun, Z.; Slesarev, A.; Alemany, L. B.; Lu, W.; Tour, J. M. Improved synthesis of graphene oxide. *ACS Nano* 2010, *4*(8), 4806–4814. DOI: 10.1021/nn1006368.

[9] Zhang, H.; Lv, X.; Li, Y.; Wang, Y.; Li, J. P25-graphene composite as a high performance photocatalyst. *ACS Nano* 2010, *4*(1), 380–386. DOI: 10.1021/nn901221k.

[10] Williamson, G. K.; Hall, W. H. X-ray line broadening from filed aluminium and wolfram. *Acta Metallurgica* 1953, *1*(1), 22–31. DOI: 10.1016/0001-6160(53)90006-6

[11] Bahari Molla Mahaleh, Y.; Sadrnezhaad, S. K.; Hosseini, D. NiO nanoparticles synthesis by chemical precipitation and effect of applied surfactant on distribution of particle size. *Journal of Nanomaterials* 2008, *2008*, Article 470595. DOI: 10.1155/2008/470595.

[12] Makuła, P.; Pacia, M.; Macyk, W. How to correctly determine the band gap energy of modified semiconductor photocatalysts based on UV–Vis spectra. *The Journal of Physical Chemistry Letters* 2018, *9*(23), 6814–6817. DOI: 10.1021/acs.jpclett.8b02892.